Supplementary Information

Normalizing tumor microenvironment with nanomedicine and metronomic therapy to improve immunotherapy

Fotios Mpekris, Chrysovalantis Voutouri, Myrofora Panagi, James W. Baish, Rakesh K. Jain and Triantafyllos Stylianopoulos

Cell culture. 4T1 (ATCC® CRL-2539™) mouse breast adenocarcinoma cell line was purchased from ATCC. The cells were maintained at 37 °C/5% CO_2 in Roswell Park Memorial Institute medium (RPMI-1640, LM-R1637, biosera) supplemented with 10% fetal bovine serum (FBS, FB-1001H, biosera) and 1% antibiotics (A5955, Sigma). The MCA205, mouse fibrosarcoma cell line was purchased from Millipore (SCC173, Millipore) and cultured in expansion medium consisting of Roswell Park Memorial Institute medium (RPMI-1640, LM-R1637, biosera) containing 2 mM L-glutamine (TMS-002-C, Sigma), 1 mM sodium pyruvate (TMS-005-C, Sigma), 10% fetal bovine serum (FBS, FB-1001H, biosera), 1x non-essential amino acids (TMS-001-C, Sigma), 1% antibiotics (A5955, Sigma) and 1x β-mercaptoethanol (ES-007-E, Sigma).

Syngeneic tumor models. A breast orthotopic syngeneic tumor model was generated by implantation of 5×10^4 4T1 cancer cells in 40 μl of serum-free medium into the third mammary fat pad of 6-8-week-old BALB/c female mice. A fibrosarcoma syngeneic tumor model was generated by implantation of 2.5×10^5 MCA205 cells in 50 μL of serum-free medium into the flank of 6-8 week old C57BL/6 male mice. Mice were purchased from the Cyprus Institute of Neurology and Genetics and all in vivo experiments were conducted in accordance with the animal welfare regulations and guidelines of the Republic of Cyprus and the European Union (European Directive 2010/63/EE and Cyprus Legislation for the protection and welfare of animals, Laws 1994-2013) under a license acquired and approved (No CY/EXP/PR.L2/2018, CY/EXP/PR.L14/2019, CY/EXP/PR.L15/2019, CY/EXP/PR.L03/2020) by the Cyprus Veterinary Services, the Cyprus national authority for monitoring animal research.

Drugs and reagents. Doxil (Pegylated liposomal doxorubicin, Janssen Pharmaceuticals) was purchased as already made solution (2 mg/ml). The immune checkpoint inhibitor (ICI) mouse monoclonal aPDL1 was purchased from BioXCell.

Interstitial Fluid Pressure IFP. Before the end of the experiment, animals were anesthetized by i.p. injection of Avertin (200 mg/kg) and interstitial fluid pressure (IFP) was measured using the wick-in-needle technique [1].

Tumor Opening experiment for quantification of growth-induced stress. Upon excision, we cut the tumors along their longest axis at approximately 80% of their thickness. We then allowed tumors to relax and measured the formed distance (tumor opening) between the two hemispheres [2]. Representative image of experimental procedure is given in Supplementary Figure S4A.

Description of the mathematical model

The mathematical model has been described in detail in our previous work [3, 4] for the study of metronomic chemotherapy and has been extended here to account for the delivery of nanomedicine. Nanomedicines have been modeled as nanocarriers that contain molecules of chemotherapy and are released at a constant release rate. Nanoparticles and chemotherapy can extravasate from the pores of the vessel walls, diffuse into the tumor interstitial space, bind to cancer cells and get internalized by the cells [5, 6]. The equations for drug delivery that are being solved by the model for delivery of chemotherapy have the form:

Delivery of chemotherapy	
$$\frac{\partial c_f}{\partial t} + \nabla \cdot \left(c_f \mathbf{v}^f \right) = D_f \nabla^2 c_f + Q_{sta} - \frac{k_{on} c_e c_f}{\Phi} + k_{off} c_b ,$$ $$\frac{\partial c_b}{\partial t} + \nabla \cdot \left(c_b \mathbf{v}^s \right) = \frac{k_{on} c_e c_f}{\Phi} - k_{off} c_b - k_{int} c_{int} ,$$ $$\frac{\partial c_{int}}{\partial t} + \nabla \cdot \left(c_{int} \mathbf{v}^s \right) = k_{int} c_b ,$$	(1)

where we assumed that chemotherapy affects the growth of the tumor by killing cancer cells but has no effect on endothelial cells and the tumor vascular density. The chemotherapeutic agent can

exist in three distinct states: free to travel in the interstitial space (c_f), bind to cancer cells (c_b), and internalized by cells (c_{int}). D_f is the diffusion coefficient of the drug, k_{on}, k_{off} and k_{int} are the association (binding), dissociation and internalization rate constants of the drug to cancer cells, c_e is the concentration of cell surface receptors, Φ is the volume fraction of tumor accessible to the drug, $\mathbf{v}^s$ and $\mathbf{v}^f$ are the velocities of solid and fluid phase respectively and Q_{sta} is the amount of drug that extravasates from the vessels into the tumor and is given later by Eq. 7.

Supplementary Table S1 depicts all model parameters employed by the model as well as their values.

In the case of the delivery of a nanoparticle carrier (c_n) containing the chemotherapy, the drug transport equations take the form:

(A) Delivery of nanomedicine (without binding)	
$$\frac{\partial c_n}{\partial t} + \nabla \cdot \left(c_n \mathbf{v}^f \right) = D_n \nabla^2 c_n + Q_{sta} - k_{rel} c_n$$ $$\frac{\partial c_f}{\partial t} + \nabla \cdot \left(c_f \mathbf{v}^f \right) = D_f \nabla^2 c_f + a k_{rel} c_n - k_{\text{int}} c_f$$ $$\frac{\partial c_{int}}{\partial t} = k_{int} c_f$$	(2)
(B) Delivery of nanomedicine (with binding)	
$$\frac{\partial c_n}{\partial t} + \nabla \cdot \left(c_n \mathbf{v}^f \right) = D_n \nabla^2 c_n + Q_{sta} - k_{rel} c_n - k_{on} c_n + k_{off} c_{nb}$$ $$\frac{\partial c_{nb}}{\partial t} = k_{on} c_n - k_{rel} c_{nb} - k_{off} c_{nb}$$ $$\frac{\partial c_f}{\partial t} + \nabla \cdot \left(c_f \mathbf{v}^f \right) = D_f \nabla^2 c_f + a k_{rel} (c_n + c_{nb}) - k_{\text{int}} c_f - k_{off} c_{nb}$$ $$\frac{\partial c_{int}}{\partial t} = k_{int} c_f$$	(3)

where c_{nb} is the concentration of nanoparticles that binds to cancer cells, D_n and D_f are the diffusion coefficients of the nanoparticle and chemotherapy, respectively, in the tumor interstitial space, k_{rel} is the release rate constant of chemotherapy form the nanoparticle and α is the number of chemotherapy molecules contained in the nanocarrier . The interstitial fluid velocity $\mathbf{v}^f$ depends on

the interstitial hydraulic conductivity k_{th} and the interstitial fluid pressure gradient, given by Darcy's law:

$$v^f = -k_{th}\nabla p_i \tag{4}$$

Combining Darcy's law with the continuity equation ($\nabla \cdot v^f = Q$) yields the steady-state fluid transport model [7]:

$$-k_{th}\nabla^2 p_i = Q \tag{5}$$

where Q denotes the fluid flux entering from the blood vessels into the tumor or the surrounding normal tissue minus the fluid flux exiting through lymphatic vessels [7]:

$$Q = L_p S_v \left(p_v - p_i \right) - L_{pl} S_{vl} \left(p_i - p_l \right) \tag{6}$$

where L_p, S_v and p_v are the hydraulic conductivity, vascular density and vascular pressure, respectively, L_{pl}, S_{vl} and p_l are the corresponding quantities for lymphatic vessels, and p_i is the interstitial fluid pressure.

The term Q_{sta} on the right hand side of Eqs. (1-3) denotes the transport of the drug across the tumor vessel wall and is given by Starling's approximation [8]:

$$Q_{sta} = P \cdot S_V \left(C_{iv} - c_n \right) + L_p S_V \left(p_V - p_i \right)\left(1 - \sigma_f \right) C_{iv} \tag{7}$$

C_{iv} is the vascular concentration of the nanoparticle and is taken to be $Civ = exp(-(t-t_0)/k_d)$ describing a bolus injection, with t_0 the time of drug injection and k_d the blood circulation decay of nanoparticle, σ_f is the reflection coefficient and P is the vascular permeability. The parameters P, L_p and σ_f that govern the transvascular transport (i.e., extravasation rate) of the nanoparticles across the tumor vessel walls are calculated as a function of the size of the pores of the vessel walls

and the size of the nanoparticle accounting for steric and hydrodynamic interactions among the particles and the vessel walls by [9]:

$$P = \frac{\gamma H D_0}{L} \tag{8}$$

where γ is the fraction of vessel wall surface area occupied by pores, H is a parameter describing hydrodynamic and steric interactions that hinder the diffusive transport of the nanoparticle through the pores of the vessel wall, L is the thickness of the vessel wall and D_0 is the diffusion coefficient of a article in free solution at 310K, given by the Stokes-Einstein relationship:

$$D_0 = \frac{K_b T}{6\pi\eta r_s} \quad , \tag{9}$$

where K_b is the Boltzmann constant, T is temperature, η is the viscosity of blood and r_s the radius of the nanoparticle.

The hydraulic conductivity of the vessel wall was calculated from the expression [9]:

$$L_p = \frac{\gamma r_0^2}{8\eta L}, \tag{10}$$

where r_0 is the pore radius.

The reflection coefficient is given by the equation [9]:

$$\sigma_f = 1 - W \tag{11}$$

where W describes hydrodynamic and steric interactions that hinder the convective transport of the nanoparticle through the pores of the vessel walls.

Ignoring electrostatic interactions, H and W are reduced to [9]:

$$H = \frac{6\pi F}{K_t} \tag{12}$$

$$W = \frac{F(2-F)K_s}{2K_t} \tag{13}$$

where F is the partition coefficient [9]:

$$F = (1-\lambda)^2 \tag{14}$$

and λ is the ratio of the drug size to the vessel wall pore size.

The coefficients K_s and K_t are determined by:

$$\begin{pmatrix} K_t \\ K_s \end{pmatrix} = \frac{9}{4}\pi^2\sqrt{2}\left(1-\lambda\right)^{-5/2}\left[1+\sum_{n=1}^{2}\begin{pmatrix} a_n \\ b_n \end{pmatrix}\left(1-\lambda\right)^n\right]+\sum_{n=0}^{4}\begin{pmatrix} a_{n+3} \\ b_{n+3} \end{pmatrix}\lambda^n \tag{15}$$

Cancer cell proliferation

The mathematical model accounts for the growth of a spherical tumor surrounded by normal tissue. To calculate the growth rate of the tumor we took into account three types of cancer cells: non-stem cancer cell (CC), stem-cell-like cancer cell (CSC) and induced cancer cell (ICC) proliferation, as well as tumor oxygenation [10-14]. In particular, to calculate the growth stretch ratio λ_g we used the expression

$$\frac{d\lambda_g}{dt} = \frac{1}{3}\left(\frac{T}{T_{tot}}S_T^c + \frac{C_{sc}}{T_{tot}}S_{C_{sc}}^c + \frac{I}{T_{tot}}S_I^c\right)\lambda_g\,, \tag{16}$$

where T is the CC population, C_{sc} is the CSC population, I is the ICC population, T_{tot} is the total density of cells given by the sum of the three populations, and S_T^c, S_{Csc}^c and S_I^c are the proliferation/degradation rates of CCs, CSCs and ICCs, respectively calculated as a function of oxygen [3].

Cancer cells, immune cells and Tumor Associated Macrophages (TAMs) population balance

Four types of immune cells are considered: the natural killer (NK) cells, the $CD8^+$ T-cells, the conventional $CD4^+$ T-cells and the regulatory $CD4^+$ T cells (Treg) [15-17]. The system of equations accounts for the recruitment rates of the immune cells, their inactivation by cancer cells, the inhibitory role of Treg cells as well as their death rate and interaction with cancer cells. Also, we account for two different types of TAMs, M1-like and M2-like.

The equations that describe the conservation of cancer cells, immune cells and TAMs are given below:

$$
\begin{aligned}
&\frac{\partial T}{\partial t} = \nabla\cdot(\mathrm{D}_{cell}\nabla T) + GS_{ftr}T - cNT - D + p_{CT}C_{sc} + p_{IT}I - \left(p_{TC} + p_{TI}\right)T - \lambda_{M1}M_1T \\
&\frac{\partial C_{sc}}{\partial t} = \nabla\cdot(\mathrm{D}_{cell}\nabla C_{sc}) + \alpha_{\mathrm{csc}}GS_{ftr_{\mathrm{csc}}}C_{sc} - c_{\mathrm{csc}}NC_{sc} - D_{\mathrm{csc}} + p_{TC}T + p_{IC}I - \left(p_{CT} + p_{CI}\right)C_{sc} \\
&\frac{\partial I}{\partial t} = \nabla\cdot(\mathrm{D}_{cell}\nabla I) + \alpha_I GS_{ftr_I}I - c_I NI - D_I + p_{TI}T + p_{CI}C_{sc} - \left(p_{IT} + p_{IC}\right)I \\
&\frac{\partial N}{\partial t} = \sigma_{nk} - f_{NK}N + \frac{g_{NK}T^2}{h+T^2}N - p_{im}NT - \lambda_{reg}T_{reg}N - \lambda_{M2}M_2N \\
&\frac{\partial L}{\partial t} = -m_{T8}L + \frac{j_{T8}D^2}{k_{im}+D^2}L - qLT + (r_N N + r_{C_{d4}}C_{d4})T - \lambda_{reg}T_{reg}L - \lambda_{M2}M_2L \\
&\frac{\partial C_{d4}}{\partial t} = s_{CD4} + re_{Cd4}C_{d4}\left(1 - \frac{C_{d4}}{C_{d4,\max}}\right) - \mu_{C_{d4}}C_{d4} \\
&\frac{\partial T_{reg}}{\partial t} = g_{reg}T_{reg} - m_{reg}T_{reg} \\
&\frac{\partial M_1}{\partial t} = g_{m1}M_1 - m_{m1}M_1 \\
&\frac{\partial M_2}{\partial t} = g_{m2}M_2 - m_{m2}M_2 + r_{Cvegf,M2}C_{vegf}M_2
\end{aligned}
\tag{17}
$$

where N is the density of NK cells, L is density of tumor-specific $CD8^+$ T-cells, C_{d4} is the density of conventional $CD4^+$ T-cells, T_{reg} is the density of the regulatory $CD4^+$ T cells, M_1 the density of M1-like TAMs cells, M_2 the density of M2-like TAMs cells and D_{cell} is the cancer cell diffusion coefficient. In the equations above all cell densities are a function of position and time, and the migration of different cell types relative to the tissue is neglected. G describes the proliferation of CCs, CSCs and ICCs as a function of oxygen and S_f is an expression that accounts for the fraction

of cells surviving drug treatment. c and D are the fractions of tumor cells killed by NK and $CD8^+$ T-cells, respectively. For the coefficients of the proliferation rates of CSCs and ICCs, i.e., α_{csc} and α_I, respectively, we assume that for normal oxygen levels they are equal to one so that all cancer cell types have the same proliferation as that of CCs. In hypoxic conditions, however, the proliferation of cancer cells with a stem-like phenotype increases. Thus, we assume that their proliferation increases inversely proportional to the oxygen concentration, so that as oxygen concentration approaches zero, the proliferation rates are twice as much as the rate in normal oxygen [18]. For the parameters c_{csc}, D_{csc}, c_I, and D_I that describe the killing potential of immune cells on CSCs and ICCs, we assume that they are more resistant in interactions with immune cells. According to experimental data [19], the cytotoxicity of $CD8^+$ T-cells against CSCs is taken to be 7-fold lower than that of CCs. As a result, the parameters that describe the killing of CSCs by immune cells are assumed to be the same as for the CCs but multiplied by a factor of 0.14. The rates of transfer of cancer cells from a type i to a type j are described by p_{ij} and their values were determined in [14]. Additionally, the parameter λ_{M1} denotes the tumoricidal effect of M1-like TAMs in cancer cells according to previous study [20]. f_{NK}, m_{T8} and m_{reg} are death rates of NK cells, $CD8^+$ T-cells and Treg cells respectively, g_{NK}, j_{T8} and g_{reg} are recruitment rates of immune cells, p_{im} and q are inactivation rates of immune cells by CCs, σ_{nk} is constant source of NK cells, r_N is the rate at which tumor-specific $CD8^+$ T-cells are stimulated to be produced as a result of tumor cells killed by NK cells and λ_{reg} is the inhibition term of NK cells and $CD8^+$ T-cells from Treg cells. Under anoxic conditions we used the lowest value for the activity of NK cells and $CD8^+$ T-cells reported in de Pillis et al. [15], which increased linearly to the highest value for normal oxygen conditions. The values of f_{NK} and m_{T8} are modified to depend on oxygen levels. According to experimental data [21], a 40 times decrease in oxygen concentration (from 20% to 0.5%) doubled the apoptotic rate of immune cells. Additionally s_{CD4} is the source of conventional $CD4^+$ T-cells, μ_{Cd4} is the natural death rate of conventional $CD4^+$ T-cells, re_{Cd4} is the growth rate of conventional $CD4^+$ T-cells and $C_{d4,max}$ is the maximum conventional $CD4^+$ T-cells population [22, 23]. r_{Cd4} is the stimulation rate of $CD8^+$ T-cells by conventional $CD4^+$ T-cells as mentioned previously [24-26]. The source term of conventional $CD4^+$ T-cells s_{CD4} will depend on oxygen concentration, as according to previous studies under hypoxic conditions it decreased 8 times [27]. Furthermore, a decrease of M2-like TAMs resulted in higher numbers of $CD8^+$ T-cells and NK cells, while conventional $CD4^+$ T-cells were not affected according to experimental data [28] and

these observations are described by the parameter λ_{M2}. g_{M1} and g_{M2} are the production rates of M1-like and M2-like TAMs, which depend on oxygen levels according to previous studies [28-30] showing that a decrease in hypoxia skewing TAMs polarization away from the M2- to M1-like phenotype. According to previous studies TAMs are associated with VEGF expression [28, 31, 32]. Specifically, VEGF-A overexpression correlated with higher numbers of M2-like TAMs ($r_{Cvegf,M2}$). The range of values of the model parameters are summarized in Supplementary Table S1. The above equations are rendered dimensionless by dividing the number of cells per finite element node by the initial number of cancer cells, T_0=5×10^2 cells. The initial population of cancer cells was taken to be: 98% CCs, 1% CSCs and 1% ICCs [33].

The dependence of cancer cell proliferation on the local oxygen concentration, G, is assumed to follow a Michaelis-Menten kinetic and has the form [34, 35]:

$$G = \frac{k_1 c_{ox}}{k_2 + c_{ox}}, \tag{18}$$

where k_1 and k_2 are growth rate parameters and c_{ox} is the oxygen concentration.

The parameter D denotes the fractional cell kill of tumor cells by CD8$^+$ T-cells and given by equation [15, 36]:

$$D = d_{im} \frac{\left(\frac{L}{T}\right)^{\lambda_{im}}}{s + \left(\frac{L}{T}\right)^{\lambda_{im}}} T, \tag{19}$$

where d_{im} is the saturation level of fractional tumor cell kill by CD8$^+$ T-cells, s is steepness coefficient of the tumor-CD8$^+$ T-cells competition term and λ_{im} the exponent of fractional cell kill by CD8$^+$ T-cells.

To account for the effect of drug delivery on growth, the surviving fraction of cells S_{ftr} is included in Eq. (17), so that in the absence of drugs S_{ftr} equals unity. The fraction of surviving cells with respect to drug concentration has been previously measured experimentally for doxorubicin [37], and the results were fitted to an exponential expression as a function of the internalized chemotherapy concentration c_{int}, i.e.,

$$S_{ftr} = 2*(\exp(-\omega c_{int})-0.5) \quad (20)$$

where ω is a fitting parameter which depends on the potency of the drug and it is calculated by fitting Eq. (20) to experimental data.

Biphasic formulation of the tumor's mechanical behavior

Tumor growth is modelled based on principles from continuum mechanics and particularly the multiplicative decomposition of the deformation gradient tensor (**F**). The kinematics of the tumor are decomposed into two components, the growth component ($\mathbf{F}_g$) that accounts for the growth of the tumor and the elastic component ($\mathbf{F}_e$) that accounts for mechanical interactions of the tumor with the surrounding normal tissue [38, 39]:

$$\mathbf{F} = \mathbf{F}_e \mathbf{F}_g, \quad (21)$$

The growth component is set to be homogenous and isotropic [40-42]

$$\mathbf{F}_g = \lambda_g \mathbf{I}, \quad (22)$$

where λ_g is defined in Eq. (16). The elastic component $\mathbf{F}_e$ of the deformation gradient tensor is determined from Eq. (21) as

$$\mathbf{F}_e = \mathbf{F}\ \mathbf{F}_g^{-1}. \quad (23)$$

The tumor is assumed to be composed of a solid (cancer and immune cells and extracellular matrix) and a interstitial fluid phase. The conservation of the tumor's solid and fluid phase is given by the mass balance equations [10, 13]:

$$\frac{\partial \Phi^c}{\partial t} + \nabla \cdot (\mathbf{v}^s \Phi^c) = \frac{T}{T_{tot}} S_T^c + \frac{C_{sc}}{T_{tot}} S_{\mathrm{Csc}}^c + \frac{I}{T_{tot}} S_I^c , \quad (24)$$

$$\frac{\partial \Phi^f}{\partial t} + \nabla \cdot (\mathbf{v}^f \Phi^f) = Q , \quad (25)$$

where Φ^c and Φ^f are the volume fractions of the solid and fluid phases, respectively.

According to the biphasic theory for soft tissues [43], the total stress tensor $\boldsymbol{\sigma}_{tot}$ is the sum of the fluid phase stress tensor $\boldsymbol{\sigma}^f = -p_i\mathbf{I}$ and the solid phase stress tensor $\boldsymbol{\sigma}^s$. As a result, the stress balance is written as:

$$\nabla \cdot \boldsymbol{\sigma}_{tot} = \mathbf{0} \Rightarrow \nabla \cdot (\boldsymbol{\sigma}^s - p_i \mathbf{I}) = \mathbf{0}, \tag{26}$$

where the Cauchy stress tensor of the solid phase $\boldsymbol{\sigma}^s$ is given by [44]:

$$\boldsymbol{\sigma}^s = J_e^{-1} \mathbf{F}_e \frac{\partial W}{\partial \mathbf{F}_e^T}, \tag{27}$$

Functional vascular density calculation

Vascular density is affected by the decrease in the vessel diameter caused by increased number of cancer cells [45]. Assuming that the number of cancer cells does not affect the number or length of vessels, but only their diameter, the change in vascular density due to vessel compression is expressed as:

$$S_v = \frac{d}{d_0} S_v^0 \rho_v^{EC}, \tag{28}$$

where S_{V0} is the vascular density of the host tissue, S_{V0} = 70 cm^{-1} and ρ_v^{EC} is the density of endothelial cells which is given below. Fitting experimental data [6, 45, 46] to a mathematical equation, an expression for degree of vessel compression (i.e., *d/do*) as a function of cancer cell density and solid stress levels was estimated.

Oxygen transport equation

A convection-diffusion-reaction type equation is employed for the calculation of the rate of change of oxygen in the tumor. The reaction term is related to the oxygen transferred from the vessels to the tumor, minus the amount of oxygen consumed by cells [10, 11], i.e.,

$$\frac{\partial c_{ox}}{\partial t} + \nabla \cdot \left(c_{ox} \mathbf{v}^f \right) = D_{ox} \nabla^2 c_{ox} - \frac{A_{ox} c_{ox}}{c_{ox} + k_{ox}} \Phi^C + P_{er} S_V \left(C_{iox} - c_{ox} \right), \tag{29}$$

where c_{ox} is the oxygen concentration, D_{ox} is the diffusion coefficient of oxygen in the interstitial space, A_{ox} and k_{ox} are oxygen uptake parameters, P_{er} is the vascular permeability of oxygen that describes diffusion across the tumor vessel wall and C_{iox} is the oxygen concentration in the vessels.

Endothelial cell transport equation

The flux of endothelial cells is given by the equation [47]:

$$\frac{\partial \hat{e}}{\partial t} = \nabla \cdot (D_{EC}(a1,a2)\nabla \hat{e} - x_n \hat{e} H(1-\hat{e}) C^0_{vegf} \nabla \hat{C}_{vegf} - W_{Se} x_n \hat{e} H(1-\hat{e}) C^0_S \nabla \hat{C}_S) + \frac{1}{e_0}(\lambda_1 C^0_{vegf} e_0 \hat{C}_{vegf} \hat{e} + \lambda_2 C^0_{vegf} e_0 \hat{C}_{vegf} \hat{e}) H(1-\hat{e}) - (\lambda_3 e_0 \hat{e} + \lambda_4 e_0 \hat{e}) \hat{e} \quad , \qquad (30)$$

Endothelial cell proliferation is based on VEGF and CXCL12 concentration as well as endothelial cell density. $\hat{e}$ is the dimensionless endothelial cell density. $\widehat{C_{vegf}}$ and C^0_{Vegf} are dimensionless and reference VEGF concentrations. Endothelial cell diffusion coefficient depends on Ang1 and Ang2: $D_{EC}(a_1,a_2)= D_{ec}(1+ s_1a_1)^{-a}(1+ s_2a_2)^b$ with a and b to be unity [48]. χ_n is a chemotactic term and W_{Se} is a weighting function describing the contribution of VEGF and CXCL12 on endothelial cell transport. The dimensionless concentration of the endothelial cells is calculated by division with the reference concentration $\hat{e} = \frac{e}{e_0}$. Loss terms describing killing of endothelial cells are also included. The parameters λ_1, λ_2, λ_3 and λ_4 are constant positive parameters.

Pericytes transport equation

Two populations/phenotypes of pericytes are considered: pericytes that are tightly associated with endothelial cells and assumed to be immotile and pericytes that are dissociated from endothelial cells and can be motile. Production rates of both phenotypes depends on PDGF-B concentration as well as on their own concentrations.

Immotile pericytes transport equation

The pericytes density is given by the equation [49, 50]:

$$\frac{\partial p_{cim}}{\partial t} = \beta_{p_c} \frac{p_{cim}}{1+ p_c / p^0_c} \frac{p_b H(\lambda_{p_b} p_b - c_{p_b})}{p_b + \alpha_{p_{c1}}} - \mu_{p_c} \frac{a_2 H(a_2 - a_{p_{c3}})}{a_2 + a_{p_{c2}}} p_{cim} + \alpha_{p_{c4}}(p_{cim\max} - p_{cim}), \qquad (31)$$

where p_c is the total pericytes density ($p_c=p_{cim}+p_{cm}$), p^0_c is the pericyte reference value, p_b is the PDGF-B concentration, p_{cimmax} is the carrying capacity of the immotile pericyte density, β_{pc}, λ_{pb}, c_{pb}, α_{p1}, α_{p2}, α_{p3}, α_{p4}, μ_{pc} are constant positive parameters.

Motile pericytes cells transport equation

The motile pericyte density is given by the equation [49, 50],

$$\frac{\partial p_{cm}}{\partial t} = \nabla \cdot (D_{p_c} \nabla p_{cm}) - \nabla \cdot (k_{p_c} p_{cm} \nabla p_b) - a_{p_{c4}} (p_{cim\max} - p_{cim}) + \beta_{pc} \frac{p_{cm}}{1 + p_c / p_c^0} \frac{p_b H(\lambda_{p_b} p_b - c_{p_b})}{p_b + \alpha_{p_{c1}}}$$
$$- \mu_{p_c} \frac{a_2 H(a_2 - a_{p_{c3}})}{a_2 + a_{p_{c2}}} p_{cm} - \mu_{p_{c2}} H(c_{pb} - \lambda_{p_b} p_b) p_{cm} \quad , \quad (32)$$

where k_{pc} is a chemotactic constant, D_{pc} is the diffusion coefficient of motile pericytes and μ_{pc2} is a constant positive parameter.

VEGF transport equation

VEGF concentration is determined by diffusion, production from cancer cells under hypoxic conditions and binding to endothelial cells receptors [47]. VEGF concentration is governed by the equation [47]:

$$\frac{\partial \hat{C}_{vegf}}{\partial t} = \nabla \cdot (D_{VEGF} \nabla \hat{C}_{vegf}) + \frac{\lambda_{10}}{C_{vegf}^0} G_a(\hat{c}_{ox}) T - (\lambda_{11} e^0 \hat{e} + \lambda_{12} e_0 \hat{e}_0 + \lambda_{13}) \hat{C}_{vegf} - \lambda_{CD4,Cvegf} C_{d4} \hat{C}_{vegf} \, , \quad (33)$$

Where $\widehat{C_{vegf}}$ is the dimensionless VEGF concentration calculated with division with a reference value $\widehat{C_{vegf}} = \frac{C_{vegf}}{C_{vegf}^0}$ and $\widehat{c_{ox}}$ is the dimensionless oxygen concentration normalized as: $\widehat{C_{ox}} = \frac{C_{ox}}{C_{ox}^0}$.

VEGF is assumed to be produced by cancer cells only and its production is enhanced under hypoxic conditions as described by the oxygen tension term G_a [47].

$$G_a(\widehat{c_{ox}}) = \begin{cases} 3\widehat{c_{ox}} & \text{for } 0 < \widehat{c_{ox}} < 0.5 \text{ (hypoxia)} \\ 2 - \widehat{c_{ox}} & \text{for } 0.5 < \widehat{c_{ox}} < 1 \text{ (normoxia)} \\ \widehat{c_{ox}} & \text{for } 1 < \widehat{c_{ox}} \text{ (hyperoxia)} \end{cases}$$

VEGF becomes unavailable due to binding to endothelial cells VEGF receptors and it can also diffuse in the tumor with a diffusion coefficient D_{VEGF}. λ_{10}, λ_{11}, λ_{12} and λ_{13} are positive constants. Additionally, knockout of conventional $CD4^+$ T cells resulted in overexpression of VEGF ($\lambda_{CD4,Cvegf}$) and not significant differences in Ang1-Ang2 [24].

CXCL12 transport equation

The stromal cell derived factor 1 (SDF1α) is also known as C-X-C motif chemokine 12 (CXCL12). We suggest in the model that VEGF released by hypoxic cancer cells up-regulates CXCL12 from cancer cells and that CXCL12 is also produced by endothelial cells in a VEGF dependent manner [51]. Therefore, CXCL12 is produced by both cancer cells and endothelial cells and it is also up-regulated by hypoxia and VEGF [51]. The transport of CXCL12 is governed by:

$$\frac{\partial \hat{C}_S}{\partial t} = \frac{\lambda_{10}}{C_s^o} G_a(\hat{c}_{ox})T + \frac{\lambda_{13}}{C_s^o} C_V^o \hat{C}_V H(1-\hat{e}) - \lambda_{13}\hat{C}_S \tag{34}$$

where λ_{10}, and λ_{13} are positive parameters. The dimensionless CXCL12 concentration is given by division with a reference concentration $\widehat{C_s} = \frac{C_s}{C_S^0}$.

PDGF-B transport equation

PDGF-B was assumed to be produced by endothelial cells and binds to pericytes [52]. PDGF-B concentration is governed by the equation [53]:

$$\frac{\partial p_b}{\partial t} = D_{p_b}\nabla^2 p_b + \beta_{p_b}\hat{e} - \mu_{p_b} p_b - \gamma_{p_b} p_b p_c \tag{35}$$

where β_{pd}, μ_{pb} and γ_{pb} are positive parameters, D_{pb} is the PDGF-B diffusion coefficient.

Ang1 and Ang2 transport equations

Ang1 is assumed to be produced by pericytes and Ang2 by endothelial cells, respectively. Their production is enhanced by hypoxia based on VEGF levels [48]. Angiopoietin 1(Ang1, α_1) and angiopoietin 2 (Ang2, α_2) are up-regulated by hypoxia and produced by endothelial cells.

$$\frac{\partial \hat{a}_1}{\partial t} = \frac{b_1}{a_0^1} p_c + \mu_1(1-\hat{a}_1) \tag{36}$$

$$\frac{\partial \hat{a}_2}{\partial t} = \frac{b_2}{a_2^1} G_a(\hat{c}_{ox})\hat{e}e_0 - \mu_2\hat{a}_2 \tag{37}$$

where b_1, b_2, μ_1 and μ_2 are positive constants. The dimensionless Ang1 and Ang2 are given by division with a reference concentration $\widehat{a_1} = \frac{a_1}{a_1^0}$, $\widehat{a_2} = \frac{a_2}{a_2^0}$. The oxygen tension term G_a is the same as used for VEGF and CXCL12. For the simplicity of the equations, we neglect diffusion of Ang1 and Ang2 and binding to specific Tie receptors [54, 55].

Supplementary Table S1. Parameters and their values used in the model

Parameter	Description	Value	Reference
μ	shear modulus	5.00 kPa for host tissue; 10.40 kPa for tumor	[56-58]
k	bulk modulus	6.67 kPa for host tissue; 10.40×10^{7} kPa for tumor	[56-58]
k_{th}	hydraulic conductivity	6.5×10^{-10} $m^2\cdot Pa^{-1}\cdot day^{-1}$	[58]
C_{iox}	initial oxygen concentration	0.2 $mol\cdot m^{-3}$	[59]
D_{ox}	oxygen diffusion coefficient	1.55×10^{-4} $m^2\cdot day^{-1}$	[11]
A_{ox}	oxygen uptake	2,200 $mol\cdot m^{-3}\cdot day^{-1}$	[11, 59]
k_{ox}	oxygen uptake	0.00464 $mol\cdot m^{-3}$	[11, 59]
k_2	growth rate parameter	0.0083 $mol\cdot m^{-3}$	[59]
c_e	receptor concentration	0.01 $mol\cdot m^{-3}$	[60, 61]
Φ	volume fraction of tumor accessible to drug	0.06	[60, 61]
k_{on}	binding rate	1.296×10^{6} day^{-1}	[60, 61]
k_{off}	dissociation rate	691.2 day^{-1}	[60, 61]
k_{int}	internalization rate	3.7 day^{-1}	[60, 61]
D_f	chemotherapy diffusion coefficient	8.64×10^{-6} $m^2\cdot day^{-1}$	[62]
ω	cancer cell survival constant	3.95 m^3/mol camptothecin; 0.6603 m^3/mol doxorubicin	[63, 64]
a_{csc}	stem-cell-like cell growth multiplier	range **: 1-2 [-]	[17]
a_I	induced cancer cell growth multiplier	range **: 1-2 [-]	---
k_d	blood circulation decay	0.417 day^{-1}	[65]

L_{vw}	vessel wall thickness	5×10^{-6} m	[66]
η	water viscosity at 310K	7×10^{-4} Pa·s	[66]
T_{abs}	absolute temperature	310K	---
γ	fraction of vessel wall surface area occupied by pores	1×10^{-5} [-]	[65]
c	fractional tumor cell kill by NK cells	range *: 3.23×10^{-7} - 3.23×10^{-6} $cell^{-1}\cdot day^{-1}$	[67]
d_{im}	fractional tumor cell kill by $CD8^+$ T-cells	range *: 1.43 – 7.15 day^{-1}	[67]
λ_{im}	exponent of fractional cell kill by $CD8^+$ T-cells	1.36 [-]	[67]
s	steepness coefficient of the tumor-$CD8^+$ T-cells competition term	2.73 [-]	[67]
σ_{nk}	constant source of NK cells	1.3×10^4 $cells\cdot day^{-1}$	[67]
f_{Nk}	death rate of NK cells	range **: 0.0412 - 0.0814 day^{-1}	[67]
m_{T8}	death rate of $CD8^+$ T-cells	range **: 0.02 - 0.04 day^{-1}	[67]
m_{reg}	death rate of Treg cells	0.02 day^{-1}	[16]
g_{NK}	recruitment rate of NK cells	initial***: 0.025 day^{-1}	[67]
j_{T8}	recruitment rate of $CD8^+$ T-cells	initial***: 0.0375 day^{-1}	[67]
g_{reg}	recruitment rate of Treg cells	initial***: 0.0375 day^{-1}	[16]

h	steepness coefficient of NK cell recruitment curve	2.02×10^{7} cell^{2}	[67]
p_{im}	inactivation rate of NK cells	1×10^{-7} cell$^{-1}\cdot$day^{-1}	[67]
k_{im}	steepness coefficient of $CD8^{+}$ T-cells recruitment curve	2.02×10^{7} cell^{2}	[67]
q	inactivation rate of $CD8^{+}$ T-cells	3.42×10^{-10} cell$^{-1}\cdot$day^{-1}	[67]
r	stimulation rate of $CD8^{+}$ T-cells	1.1×10^{-7} cell$^{-1}\cdot$day^{-1}	[67]
λ_{reg}	inhibition term of NK cells and $CD8^{+}$ T-cells from Treg cells	100 cell$^{-1}\cdot$day^{-1}	[16]
p_{TC}	rate of dedifferentiation from cancer cells to stem-like-cell cancer cells	0.55 day^{-1} prior treatment; 0 day^{-1} after application of chemotherapy	[14]
p_{CT}	rate of transition from stem-like-cell cancer cells to cancer cells	1 day^{-1} prior treatment; 0.96 day^{-1} after application of chemotherapy	[14]
p_{CI}	rate of transition from stem-like-cell cancer cells to induced cancer cells	0.58 day^{-1} prior treatment; 0 day^{-1} after application of chemotherapy	[14]
p_{IC}	rate of transition from induced cancer cells to stem-like-cell cancer cells	0.96 day^{-1} prior treatment; 0.38 day^{-1} after application of chemotherapy	[14]

p_{TI}	rate of transition from cancer cells to induced cancer cells	0.21 day^{-1} prior treatment; 1 day^{-1} after application of chemotherapy	[14]
p_{IT}	rate of transition from induced cancer cells to cancer cells	1 day^{-1} prior treatment; 0.98 day^{-1} after application of chemotherapy	[14]
λ_{M1}	tumoricidal effect of M1-like TAMs in cancer cells	3 s^{-1}	[20]
g_{M1}	production rate of M1-like TAMs	initial****: 0.0375 day^{-1}	[28, 29]
g_{M2}	production rate of M2-like TAMs	initial****: 0.0375 day^{-1}	[28, 29]
m_{M1}	death rate of M1-like TAMs	0.02 day^{-1}	[4]
m_{M2}	death rate of M2-like TAMs	0.02 day^{-1}	[4]
r_s	size of nanoparticle carrier	20 nm CRLX101; 100 nm DOXIL	[5, 68]
k_{el}	chemotherapy release rate	0.3 day^{-1} CRLX101; 0.181 day^{-1} DOXIL	[68, 69]
a	chemotherapy molecules contained in nanocarrier	12 CRLX101; 10000 DOXIL	[70, 71]
k_d	blood circulation decay	1 day^{-1}	[68]
D_n	nanoparticle diffusion coefficient	6×10^{-7} $m^2.day^{-1}$ CRLX101; 8.64×10^{-8} $m^2.day^{-1}$ DOXIL	[62]

L	Vessel wall thickness	5×10^{-6} m	[42]
p_V	Vascular pressure	30 mmHg	[7]
η	Blood viscosity	3×10^{-5} mmHg·s	[42]
γ	Fraction of vessel wall surface area occupied by pores	5×10^{-4} [-]	[72]
a_1	Coefficient for K_t	−73/60 [-]	[9]
a_2	Coefficient for K_t	77.293/50.400 [-]	[9]
a_3	Coefficient for K_t	−22.5083 [-]	[9]
a_4	Coefficient for K_t	−5.617 [-]	[9]
a_5	Coefficient for K_t	−0.3363 [-]	[9]
a_6	Coefficient for K_t	−1.216 [-]	[9]
a_7	Coefficient for K_t	1.647 [-]	[9]
b_1	Coefficient for K_s	7/60 [-]	[9]
b_2	Coefficient for K_s	−2.227/50.400 [-]	[9]
b_3	Coefficient for K_s	4.0180 [-]	[9]
b_4	Coefficient for K_s	−3.9788 [-]	[9]
b_5	Coefficient for K_s	−1.9215 [-]	[9]
b_6	Coefficient for K_s	4.392 [-]	[9]
b_7	Coefficient for K_s	5.006 [-]	[9]
D_{VEGF}	VEGF diffusion coefficient	$3.1\text{x}10^{-11}$ [m^2/s]	[47]
D_{ec}	Endothelial cell diffusion coefficient	$1\text{x}10^{-15}$ [m^2/s]	[48]

D_{pb}	PDGF-B diffusion coefficient	$1.65x10^{-3}$ [mm^2/h]	[50]
β_{pb}	Non-negative parameter	$1.25x10^{4}$ [1/h]	[50]
γ_{pb}	Non-negative parameter	$2.5x10^{6}$ [1/(μM.h]	[50]
μ_{pb}	Non-negative parameter	10^{-1} [1/h]	[50]
λ_{pb}	Positive parameter	100%	[50]
c_{pb}	Positive parameter	$3.33x10^{-3}$ [μM]	[50]
D_{pc}	Diffusion coefficient of motile pericyte	$1.65x10^{-3}$ [mm^2/h]	[50]
k_{pc}	Pericyte chemotactic	10^{-1} [mm^2/(μM.h)]	[50]
β_{pc}	Non-negative parameter	$1.25x10^{-1}$ [1/h]	[50]
μ_{pc}	Non-negative parameter	$4.17x10^{-2}$ [1/h]	[50]
μ_{pc2}	Non-negative parameter	$4.17x10^{-2}$ [1/h]	[50]
a_{pc1}	Positive parameter	$3.33x10^{-3}$ [μM]	[50]
a_{pc2}	Positive parameter	10^{-3} [μM]	[50]
a_{pc3}	Positive parameter	10^{-3} [μM]	[50]
a_{pc4}	Positive parameter	$4.17x10^{-3}$ [1/h]	[50]
p_c^0	Reference pericyte	$3.32x10^{-8}$ [μM]	[50]

x_n	Chemotactic endothelial cell	$2x10^{-15}$ [m^5/kg-s]	[47]
W_{ST}	Weight between oxygen- CXCL12	1	[47]
W_{Se}	Weight between VEGF- CXCL12	1	[47]
C_s^0	Reference CXCL12 concentration	$1x10^{-3}$ [g/m^3]	[47]
C_{vegf}^0	Reference VEGF concentration	$1x10^{-3}$ [g/cm^3]	[47]
e^0	Reference value of endothelial cell	$1x10^{-3}$ [g/cm^3]	[47]
a_1^0	Reference a_1 concentration	$1x10^{-3}$ [g/cm^3]	[48]
a_2^0	Reference a_2 concentration	$1x10^{-3}$ [g/cm^3]	[48]
s_{CD4}	source term of conventional $CD4^+$ T- cells	150 day^{-1}**	[22]
μ_{Cd4}	natural death rate of conventional $CD4^+$ T-cells	0.02 day^{-1}	[22]
re_{Cd4}	the growth rate of conventional $CD4^+$ T-cells	0.03 day^{-1}	[22]
r_{Cd4}	stimulation rate of $CD8^+$ T cells by	$1x10^{-15}$ $cells^{-1}.day^{-1}$	(23)

	conventional $CD4^+$ T-cells		
λ_4	Positive parameters	$1x10^{-1}$ [cm^3/g-s]	[47]
λ_5	Positive parameters	$5.56x10^{-7}$[1/s]	[47]
λ_{10}	Positive parameters	$6.8x10^{-3}$ [1/s]	[47]
λ_{11}	Positive parameters	4 [cm^3/g-s]	[47]
λ_{12}	Positive parameters	4 [cm^3/g-s]	[47]
λ_{13}	Positive parameters	$4x10^{-5}$ [1/s]	[47]
b_1	Positive parameters	2280 [1/h]	[48]
b_2	Positive parameters	18240 [1/h]	[48]
μ_1	Positive parameters	456 [1/h]	[48]
μ_2	Positive parameters	456 [1/h]	[48]
s_1	Positive parameters	$1x10^3$ [cm^3/ g]	[48]
s_2	Positive parameters	$1x10^3$ [cm^3/ g]	[48]

*: linear increase from minimum to maximum value depending on oxygen levels

**: linear decrease from maximum to minimum value depending on oxygen levels

***: initial value in the absence of drug.

****: initial value in normoxia conditions.

Supplementary Table S2. Value of parameter k_1 used for fitting the model to the two experimental studies. The parameter k_1 describes the dependence of cancer cell proliferation on the local oxygen concentration (Eq. 18).

Experimental study	k_1
Pham et al. [73]	0.47 day^{-1}
Conley et al. [74]	0.77 day^{-1}

Supplementary Figure S1. Representative time intensity curves for **(A)** Control group and **(B)** Doxil (2 mg/kg) group on Day18 (end of 1st treatment cycle) and definition of parameters measured: PI (peak intensity), AUC (area under the curve), rise time and mean transit time. According to previous studies [75, 76], i) peak intensity and area under the curve are related to blood volume and ii) rise time and mean transit time are related to blood flow/perfusion. Black dots are the raw data and the red line is the fit to the data for the calculation of the parameters measured.

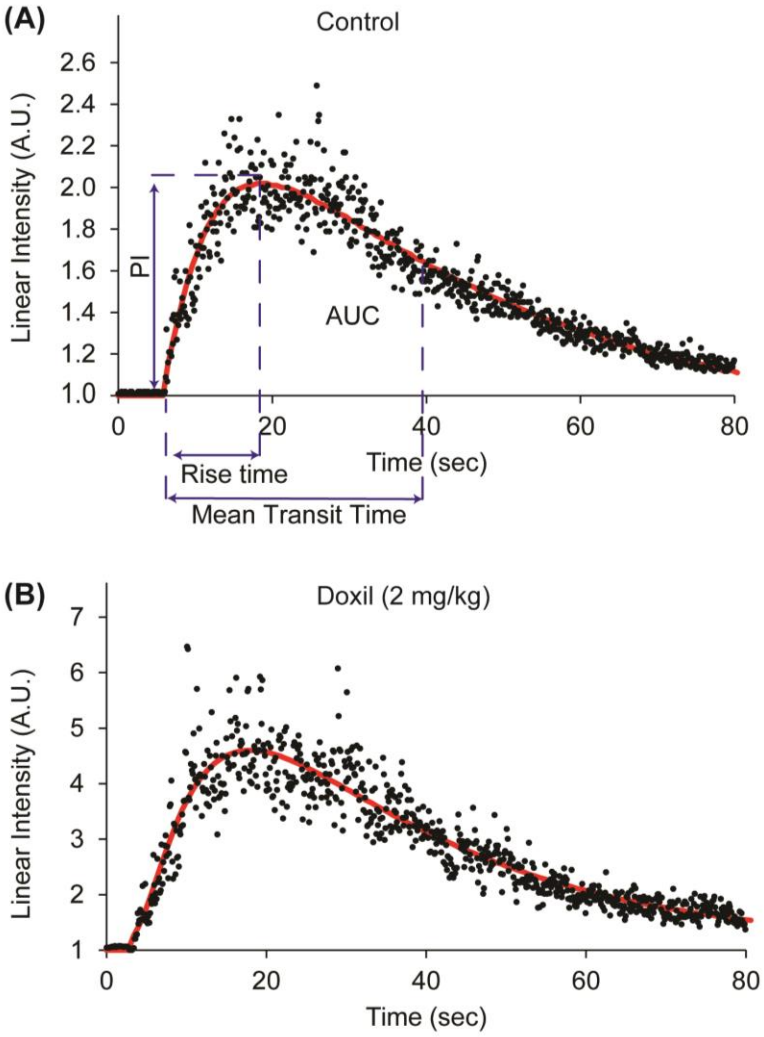

Supplementary Figure S2. Low and more frequent doses of Doxil (1 mg/kg and 2 mg/kg) combined with aPDL1 treatment result in a higher peak intensity of contrast enhanced ultrasound agents (i.e. microbubbles) -measured with ultrasound- compared with control, aPDL1 alone and group with high but less frequent doses of Doxil 6 mg/kg combined with ICB aPDL1. No effect is observed in the total integrated contrast enhancement, measured by the area under the time-intensity curve (AUC). Statistical analyses were performed by comparing the Doxil 1 mg/kg and Doxil 2 mg/kg with all other treatment groups *, $p \leq 0.05$, determined by t-test. Data presented as mean ± SEM (n = 6 mice per group).

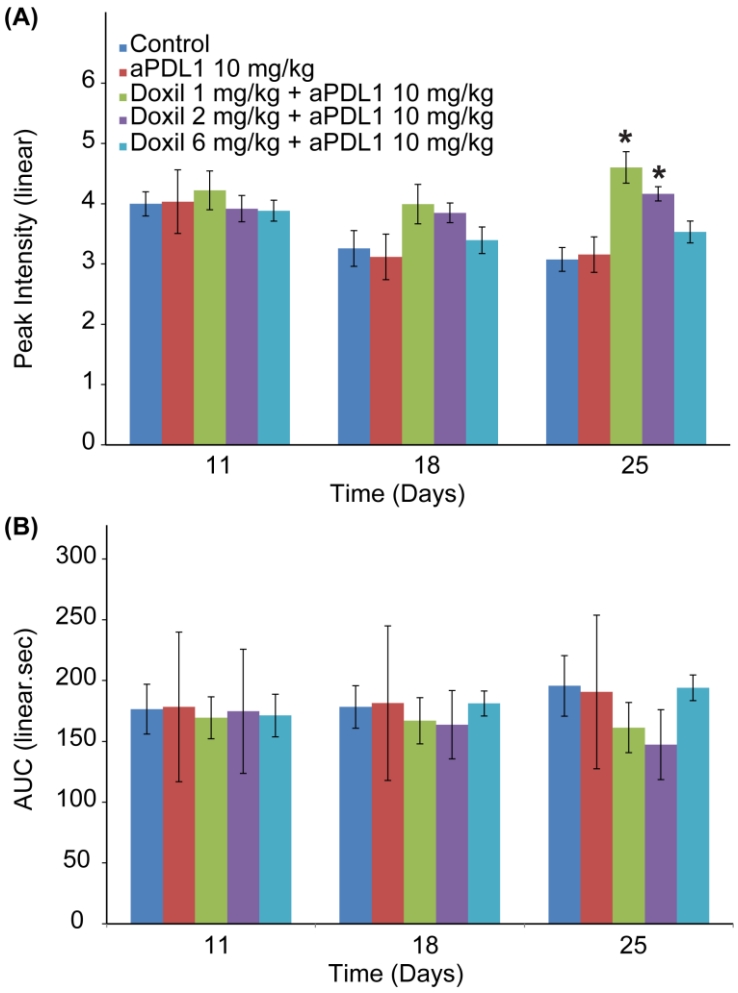

Supplementary Figure S3. Low and more frequent doses of the nanomedicine Doxil normalize the tumor mechanical microenvironment in MCA205 tumors. **(A)** Quantification of the average elastic modulus of the tumors on Days 11, 18 and 25 using SWE. **(B)** Mean transit time, **(C)** rise time, **(D)** peak intensity and **(E)** area under the time-intensity curve (AUC) of contrast agents for the different treatment groups using DCEUS. **(F)** Interstitial fluid pressure (IFP) levels at the end of the treatment protocol. Statistical analyses were performed by comparing the Doxil 6 mg/kg group with the control and aPDL1 groups * and the Doxil 1 mg/kg and Doxil 2 mg/kg with all other treatment groups **, $p \leq 0.05$, determined by t-test. Data presented as mean ± SEM (n = 6 mice per group).

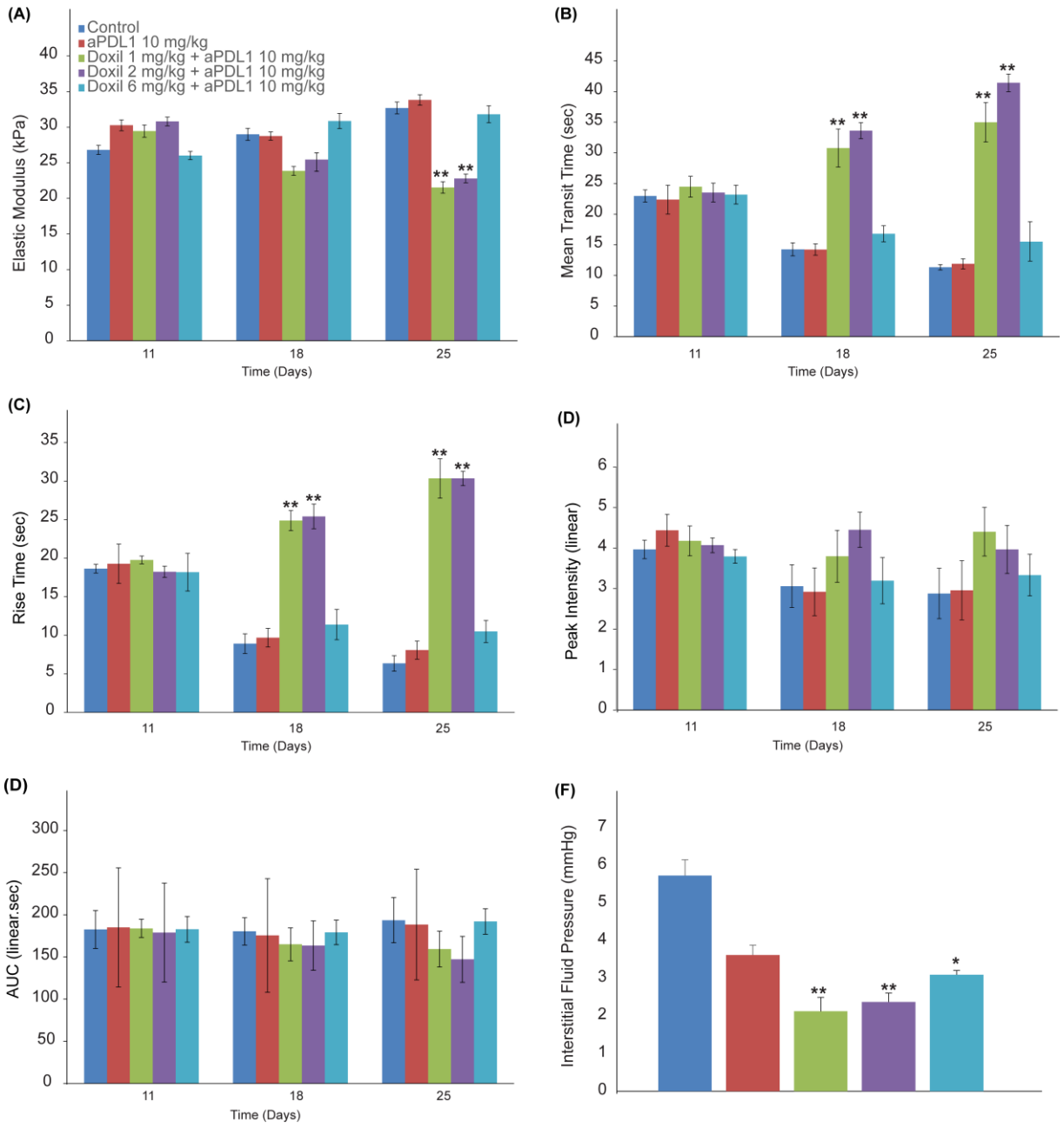

Supplementary Figure S4. (A) Representative image showing the opening of the tumor after a tumor opening experiment as a measure of growth-induced, residual stress. After tumor excision, a cut was made ~80% of the thickness of tumor along the main axis and the tumor opens up as a result of stress release and tissue relaxation. Measurements of tumor opening in **(B)** 4T1 and **(C)** MCA205 tumors, indicating that treatment with low and more frequent doses of Doxil (1 mg/kg and 2 mg/kg) combined with aPDL1 treatment leads to lower values of tumor relaxation compared to control, aPDL1 alone and the 6 mg/kg Doxil group, resulting in lower levels of growth-induced stress**.** Furthermore, the tumor opening decreases significantly in the 6 mg/kg Doxil group compared to control and aPDL1 monotherapy groups. Statistical analyses were performed by comparing the Doxil 6 mg/kg group with the control or aPDL1 monotherapy groups * and the Doxil 1 mg/kg and Doxil 2 mg/kg with all other treatment groups **, $p \leq 0.05$, determined by t-test. Data presented as mean ± SEM (n = 6 mice per group).

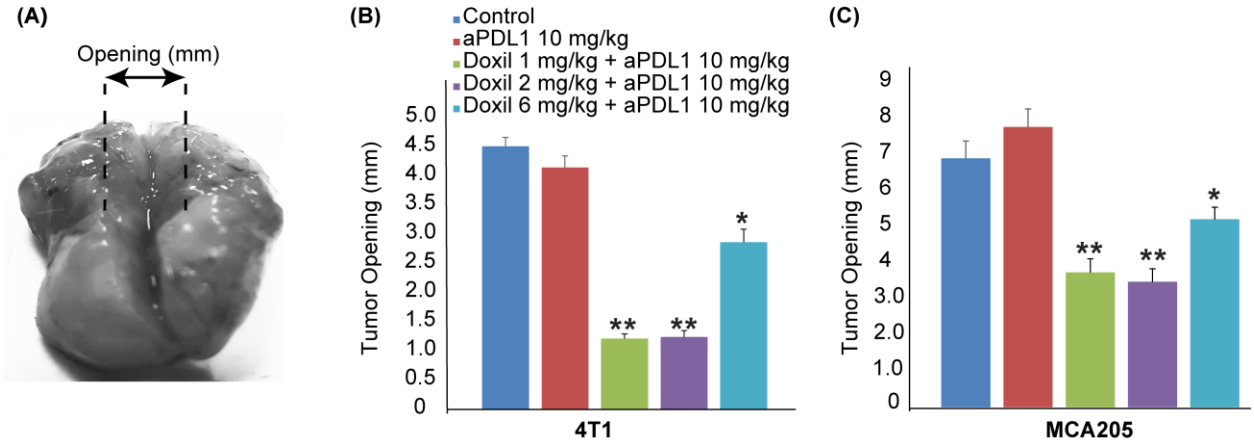

References

[1] H.O. Fadnes, R.K. Reed, K. Aukland, Interstitial fluid pressure in rats measured with a modified wick technique, Microvascular research, 14 (1977) 27-36.
[2] T. Stylianopoulos, J.D. Martin, V.P. Chauhan, S.R. Jain, B. Diop-Frimpong, N. Bardeesy, B.L. Smith, C.R. Ferrone, F.J. Hornicek, Y. Boucher, L.L. Munn, R.K. Jain, Causes, consequences, and remedies for growth-induced solid stress in murine and human tumors, Proceedings of the National Academy of Sciences of the United States of America, 109 (2012) 15101-15108.
[3] F. Mpekris, J.W. Baish, T. Stylianopoulos, R.K. Jain, Role of vascular normalization in benefit from metronomic chemotherapy, Proceedings of the National Academy of Sciences of the United States of America, 114 (2017) 1994-1999.
[4] F. Mpekris, C. Voutouri, J.W. Baish, D.G. Duda, L.L. Munn, T. Stylianopoulos, R.K. Jain, Combining microenvironment normalization strategies to improve cancer immunotherapy, Proceedings of the National Academy of Sciences of the United States of America, 117 (2020) 3728-3737.
[5] T. Stylianopoulos, E.A. Economides, J.W. Baish, D. Fukumura, R.K. Jain, Towards Optimal Design of Cancer Nanomedicines: Multi-stage Nanoparticles for the Treatment of Solid Tumors, Annals of biomedical engineering, 43 (2015) 2291-2300.
[6] F. Mpekris, S. Angeli, A.P. Pirentis, T. Stylianopoulos, Stress-mediated progression of solid tumors: effect of mechanical stress on tissue oxygenation, cancer cell proliferation, and drug delivery, Biomechanics and modeling in mechanobiology, 14 (2015) 1391-1402.
[7] L.T. Baxter, R.K. Jain, Transport of fluid and macromolecules in tumors. I. Role of interstitial pressure and convection, Microvascular research, 37 (1989) 77-104.
[8] T. Stylianopoulos, L.L. Munn, R.K. Jain, Reengineering the Physical Microenvironment of Tumors to Improve Drug Delivery and Efficacy: From Mathematical Modeling to Bench to Bedside, Trends in cancer, 4 (2018) 292-319.
[9] W.M. Deen, Hindered Transport of Large molecules in Liquid-Filled Pores, AIChE J, 33 (1987) 1409-1425.
[10] T. Roose, P.A. Netti, L.L. Munn, Y. Boucher, R.K. Jain, Solid stress generated by spheroid growth estimated using a linear poroelasticity model, Microvasc Res, 66 (2003) 204-212.
[11] Y. Kim, M.A. Stolarska, H.G. Othmer, The role of the microenvironment in tumor growth and invasion, Prog Biophys Mol Bio, 106 (2011) 353-379.
[12] J. MacLaurin, J. Chapman, G.W. Jones, T. Roose, The buckling of capillaries in solid tumours, P Roy Soc a-Math Phy, 468 (2012) 4123-4145.
[13] C. Voutouri, T. Stylianopoulos, Evolution of osmotic pressure in solid tumors, J Biomech, (2014).
[14] A. Goldman, B. Majumder, A. Dhawan, S. Ravi, D. Goldman, M. Kohandel, P.K. Majumder, S. Sengupta, Temporally sequenced anticancer drugs overcome adaptive resistance by targeting a vulnerable chemotherapy-induced phenotypic transition, Nature communications, 6 (2015) 6139.
[15] L.G. de Pillis, A.E. Radunskaya, C.L. Wiseman, A validated mathematical model of cell-mediated immune response to tumor growth, Cancer research, 65 (2005) 7950-7958.
[16] D. Fouchet, R. Regoes, A population dynamics analysis of the interaction between adaptive regulatory T cells and antigen presenting cells, PloS one, 3 (2008) e2306.
[17] N.J. Burroughs, B.M.P.M. Oliveira, A.A. Pinto, M. Ferreira, Immune response dynamics, Math Comput Model, 53 (2011) 1410-1419.
[18] S.J. Conley, E. Gheordunescu, P. Kakarala, B. Newman, H. Korkaya, A.N. Heath, S.G. Clouthier, M.S. Wicha, Antiangiogenic agents increase breast cancer stem cells via the generation

of tumor hypoxia, Proceedings of the National Academy of Sciences of the United States of America, 109 (2012) 2784-2789.
[19] M. Todaro, M. D'Asaro, N. Caccamo, F. Iovino, M.G. Francipane, S. Meraviglia, V. Orlando, C. La Mendola, G. Gulotta, A. Salerno, F. Dieli, G. Stassi, Efficient killing of human colon cancer stem cells by gammadelta T lymphocytes, Journal of immunology, 182 (2009) 7287-7296.
[20] G. Mahlbacher, L.T. Curtis, J. Lowengrub, H.B. Frieboes, Mathematical modeling of tumor-associated macrophage interactions with the cancer microenvironment, Journal for immunotherapy of cancer, 6 (2018) 10.
[21] I.B. Barsoum, C.A. Smallwood, D.R. Siemens, C.H. Graham, A mechanism of hypoxia-mediated escape from adaptive immunity in cancer cells, Cancer research, 74 (2014) 665-674.
[22] A.S. Perelson, D.E. Kirschner, R. De Boer, Dynamics of HIV infection of CD4+ T cells, Mathematical biosciences, 114 (1993) 81-125.
[23] R.V. Culshaw, S. Ruan, A delay-differential equation model of HIV infection of CD4(+) T-cells, Mathematical biosciences, 165 (2000) 27-39.
[24] L. Tian, A. Goldstein, H. Wang, H. Ching Lo, I. Sun Kim, T. Welte, K. Sheng, L.E. Dobrolecki, X. Zhang, N. Putluri, T.L. Phung, S.A. Mani, F. Stossi, A. Sreekumar, M.A. Mancini, W.K. Decker, C. Zong, M.T. Lewis, X.H. Zhang, Mutual regulation of tumour vessel normalization and immunostimulatory reprogramming, Nature, 544 (2017) 250-254.
[25] M. De Palma, R.K. Jain, CD4+ T Cell Activation and Vascular Normalization: Two Sides of the Same Coin?, Immunity, 46 (2017) 773-775.
[26] L. de Pillis, T. Caldwell, E. Sarapata, H. Williams, Mathematical Modeling of Regulatory T Cell Effects on Renal Cell Carcinoma Treatment, Discrete Cont Dyn-B, 18 (2013) 915-943.
[27] Q. Wang, C. Liu, F. Zhu, F. Liu, P. Zhang, C. Guo, X. Wang, H. Li, C. Ma, W. Sun, Y. Zhang, W. Chen, L. Zhang, Reoxygenation of hypoxia-differentiated dentritic cells induces Th1 and Th17 cell differentiation, Molecular immunology, 47 (2010) 922-931.
[28] C. Rolny, M. Mazzone, S. Tugues, D. Laoui, I. Johansson, C. Coulon, M.L. Squadrito, I. Segura, X. Li, E. Knevels, S. Costa, S. Vinckier, T. Dresselaer, P. Akerud, M. De Mol, H. Salomaki, M. Phillipson, S. Wyns, E. Larsson, I. Buysschaert, J. Botling, U. Himmelreich, J.A. Van Ginderachter, M. De Palma, M. Dewerchin, L. Claesson-Welsh, P. Carmeliet, HRG inhibits tumor growth and metastasis by inducing macrophage polarization and vessel normalization through downregulation of PlGF, Cancer cell, 19 (2011) 31-44.
[29] Y. Huang, M. Snuderl, R.K. Jain, Polarization of tumor-associated macrophages: a novel strategy for vascular normalization and antitumor immunity, Cancer cell, 19 (2011) 1-2.
[30] Y. Huang, S. Goel, D.G. Duda, D. Fukumura, R.K. Jain, Vascular normalization as an emerging strategy to enhance cancer immunotherapy, Cancer research, 73 (2013) 2943-2948.
[31] N. Linde, W. Lederle, S. Depner, N. van Rooijen, C.M. Gutschalk, M.M. Mueller, Vascular endothelial growth factor-induced skin carcinogenesis depends on recruitment and alternative activation of macrophages, The Journal of pathology, 227 (2012) 17-28.
[32] C. Stockmann, A. Doedens, A. Weidemann, N. Zhang, N. Takeda, J.I. Greenberg, D.A. Cheresh, R.S. Johnson, Deletion of vascular endothelial growth factor in myeloid cells accelerates tumorigenesis, Nature, 456 (2008) 814-818.
[33] P.C. Hermann, S.L. Huber, T. Herrler, A. Aicher, J.W. Ellwart, M. Guba, C.J. Bruns, C. Heeschen, Distinct populations of cancer stem cells determine tumor growth and metastatic activity in human pancreatic cancer, Cell stem cell, 1 (2007) 313-323.
[34] J.J. Casciari, S.V. Sotirchos, R.M. Sutherland, Mathematical-Modeling of Microenvironment and Growth in Emt6/Ro Multicellular Tumor Spheroids, Cell Proliferat, 25 (1992b) 1-22.

[35] J.J. Casciari, S.V. Sotirchos, R.M. Sutherland, Variations in Tumor-Cell Growth-Rates and Metabolism with Oxygen Concentration, Glucose-Concentration, and Extracellular Ph, J Cell Physiol, 151 (1992a) 386-394.
[36] O. Milberg, C. Gong, M. Jafarnejad, I.H. Bartelink, B. Wang, P. Vicini, R. Narwal, L. Roskos, A.S. Popel, A QSP Model for Predicting Clinical Responses to Monotherapy, Combination and Sequential Therapy Following CTLA-4, PD-1, and PD-L1 Checkpoint Blockade, Scientific reports, 9 (2019) 11286.
[37] D.J. Kerr, A.M. Kerr, R.I. Freshney, S.B. Kaye, Comparative Intracellular Uptake of Adriamycin and 4'-Deoxydoxorubicin by Non-Small Cell Lung-Tumor Cells in Culture and Its Relationship to Cell-Survival, Biochem Pharmacol, 35 (1986) 2817-2823.
[38] E.K. Rodriguez, A. Hoger, A.D. McCulloch, Stress-dependent finite growth in soft elastic tissues, Journal of biomechanics, 27 (1994) 455-467.
[39] R. Skalak, S. Zargaryan, R.K. Jain, P.A. Netti, A. Hoger, Compatibility and the genesis of residual stress by volumetric growth, Journal of mathematical biology, 34 (1996) 889-914.
[40] T. Roose, P.A. Netti, L.L. Munn, Y. Boucher, R.K. Jain, Solid stress generated by spheroid growth estimated using a linear poroelasticity model, Microvascular research, 66 (2003) 204-212.
[41] Y. Kim, M.A. Stolarska, H.G. Othmer, The role of the microenvironment in tumor growth and invasion, Progress in biophysics and molecular biology, 106 (2011) 353-379.
[42] T. Stylianopoulos, J.D. Martin, M. Snuderl, F. Mpekris, S.R. Jain, R.K. Jain, Coevolution of solid stress and interstitial fluid pressure in tumors during progression: Implications for vascular collapse, Cancer research, 73 (2013) 3833-3841.
[43] V.C. Mow, S.C. Kuei, W.M. Lai, C.G. Armstrong, Biphasic Creep and Stress-Relaxation of Articular-Cartilage in Compression - Theory and Experiments, J Biomech Eng-T Asme, 102 (1980) 73-84.
[44] L.A. Taber, Theoretical study of Beloussov's hyper-restoration hypothesis for mechanical regulation of morphogenesis, Biomechanics and modeling in mechanobiology, 7 (2008) 427-441.
[45] G. Griffon-Etienne, Y. Boucher, C. Brekken, H.D. Suit, R.K. Jain, Taxane-induced apoptosis decompresses blood vessels and lowers interstitial fluid pressure in solid tumors: clinical implications, Cancer research, 59 (1999) 3776-3782.
[46] T.P. Padera, B.R. Stoll, J.B. Tooredman, D. Capen, E. di Tomaso, R.K. Jain, Pathology: cancer cells compress intratumour vessels, Nature, 427 (2004) 695.
[47] R.C. Schugart, A. Friedman, R. Zhao, C.K. Sen, Wound angiogenesis as a function of tissue oxygen tension: a mathematical model, Proceedings of the National Academy of Sciences of the United States of America, 105 (2008) 2628-2633.
[48] M.J. Plank, B.D. Sleeman, P.F. Jones, The role of the angiopoietins in tumour angiogenesis, Growth factors, 22 (2004) 1-11.
[49] X.M. Zheng, G.Y. Koh, T. Jackson, A Continuous Model of Angiogenesis: Initiation, Extension, and Maturation of New Blood Vessels Modulated by Vascular Endothelial Growth Factor, Angiopoietins, Platelet-Derived Growth Factor-B, and Pericytes, Discrete Cont Dyn-B, 18 (2013) 1109-1154.
[50] L.G. Hutchinson, E.A. Gaffney, P.K. Maini, J. Wagg, A. Phipps, H.M. Byrne, Vascular phenotype identification and anti-angiogenic treatment recommendation: A pseudo-multiscale mathematical model of angiogenesis, Journal of theoretical biology, 398 (2016) 162-180.
[51] D. Zagzag, Y. Lukyanov, L. Lan, M.A. Ali, M. Esencay, O. Mendez, H. Yee, E.B. Voura, E.W. Newcomb, Hypoxia-inducible factor 1 and VEGF upregulate CXCR4 in glioblastoma:

implications for angiogenesis and glioma cell invasion, Laboratory investigation; a journal of technical methods and pathology, 86 (2006) 1221-1232.
[52] X. Zheng, G.Y. Koh, T. Jackson, A CONTINUOUS MODEL OF ANGIOGENESIS: INITIATION, EXTENSION, AND MATURATION OF NEW BLOOD VESSELS MODULATED BY VASCULAR ENDOTHELIAL GROWTH FACTOR, ANGIOPOIETINS, PLATELET-DERIVED GROWTH FACTOR-B, AND PERICYTES, Discrete and continuous dynamical systems series B, 18 (2013) 1109-1154.
[53] X. Zheng, G.Y. Koh, T. Jackson, A continuous model of angiogenesis: initiation, extension, and maturation of new blood vessels modulated by vascular endothelial growth factor, angiopoietins, platelet-derived growth factor-B, and pericytes, Discrete & Continuous Dynamical Systems-B, 18 (2013) 1109-1154.
[54] F. Billy, B. Ribba, O. Saut, H. Morre-Trouilhet, T. Colin, D. Bresch, J.P. Boissel, E. Grenier, J.P. Flandrois, A pharmacologically based multiscale mathematical model of angiogenesis and its use in investigating the efficacy of a new cancer treatment strategy, Journal of theoretical biology, 260 (2009) 545-562.
[55] J.L. Gevertz, S. Torquato, Modeling the effects of vasculature evolution on early brain tumor growth, Journal of theoretical biology, 243 (2006) 517-531.
[56] M. Eder, S. Raith, J. Jalali, A. Volf, M. Settles, H.G. Machens, L. Kovacs, Comparison of Different Material Models to Simulate 3-D Breast Deformations Using Finite Element Analysis, Ann Biomed Eng, 42 (2014) 843-857.
[57] A. Samani, J. Zubovits, D. Plewes, Elastic moduli of normal and pathological human breast tissues: an inversion-technique-based investigation of 169 samples, Phys Med Biol, 52 (2007) 1565-1576.
[58] P.A. Netti, D.A. Berk, M.A. Swartz, A.J. Grodzinsky, R.K. Jain, Role of extracellular matrix assembly in interstitial transport in solid tumors, Cancer Res, 60 (2000) 2497-2503.
[59] J.J. Casciari, S.V. Sotirchos, R.M. Sutherland, Variations in tumor cell growth rates and metabolism with oxygen concentration, glucose concentration, and extracellular pH, Journal of cellular physiology, 151 (1992) 386-394.
[60] W. Mok, T. Stylianopoulos, Y. Boucher, R.K. Jain, Mathematical modeling of herpes simplex virus distribution in solid tumors: implications for cancer gene therapy, Clinical cancer research : an official journal of the American Association for Cancer Research, 15 (2009) 2352-2360.
[61] M.M. Schmidt, K.D. Wittrup, A modeling analysis of the effects of molecular size and binding affinity on tumor targeting, Molecular cancer therapeutics, 8 (2009) 2861-2871.
[62] A. Pluen, Y. Boucher, S. Ramanujan, T.D. McKee, T. Gohongi, E. di Tomaso, E.B. Brown, Y. Izumi, R.B. Campbell, D.A. Berk, R.K. Jain, Role of tumor-host interactions in interstitial diffusion of macromolecules: cranial vs. subcutaneous tumors, Proceedings of the National Academy of Sciences of the United States of America, 98 (2001) 4628-4633.
[63] N.K. Sharma, A. Kumar, A. Kumari, E.J. Tokar, M.P. Waalkes, C.D. Bortner, J. Williams, M. Ehrenshaft, R.P. Mason, B.K. Sinha, Nitric Oxide Down-Regulates Topoisomerase I and Induces Camptothecin Resistance in Human Breast MCF-7 Tumor Cells, PloS one, 10 (2015) e0141897.
[64] S. Eikenberry, A tumor cord model for doxorubicin delivery and dose optimization in solid tumors, Theoretical biology & medical modelling, 6 (2009) 16.
[65] V.P. Chauhan, T. Stylianopoulos, J.D. Martin, Z. Popovic, O. Chen, W.S. Kamoun, M.G. Bawendi, D. Fukumura, R.K. Jain, Normalization of tumour blood vessels improves the delivery of nanomedicines in a size-dependent manner, Nature nanotechnology, 7 (2012) 383-388.

[66] T. Stylianopoulos, J.D. Martin, M. Snuderl, F. Mpekris, S.R. Jain, R.K. Jain, Coevolution of solid stress and interstitial fluid pressure in tumors during progression: implications for vascular collapse, Cancer research, 73 (2013) 3833-3841.
[67] L.G. de Pillis, A.E. Radunskaya, C.L. Wiseman, A validated mathematical model of cell-mediated immune response to tumor growth, Cancer research, 65 (2005) 7950-7958.
[68] S. Eliasof, D. Lazarus, C.G. Peters, R.I. Case, R.O. Cole, J. Hwang, T. Schluep, J. Chao, J. Lin, Y. Yen, H. Han, D.T. Wiley, J.E. Zuckerman, M.E. Davis, Correlating preclinical animal studies and human clinical trials of a multifunctional, polymeric nanoparticle, Proceedings of the National Academy of Sciences of the United States of America, 110 (2013) 15127-15132.
[69] C. Wong, T. Stylianopoulos, J. Cui, J. Martin, V.P. Chauhan, W. Jiang, Z. Popovic, R.K. Jain, M.G. Bawendi, D. Fukumura, Multistage nanoparticle delivery system for deep penetration into tumor tissue, Proceedings of the National Academy of Sciences of the United States of America, 108 (2011) 2426-2431.
[70] J. Cheng, K.T. Khin, M.E. Davis, Antitumor activity of beta-cyclodextrin polymer-camptothecin conjugates, Molecular pharmaceutics, 1 (2004) 183-193.
[71] C.M. Dawidczyk, C. Kim, J.H. Park, L.M. Russell, K.H. Lee, M.G. Pomper, P.C. Searson, State-of-the-art in design rules for drug delivery platforms: lessons learned from FDA-approved nanomedicines, Journal of controlled release : official journal of the Controlled Release Society, 187 (2014) 133-144.
[72] V.P. Chauhan, T. Stylianopoulos, J.D. Martin, Z. Popovic, O. Chen, W.S. Kamoun, M.G. Bawendi, D. Fukumura, R.K. Jain, Normalization of tumour blood vessels improves the delivery of nanomedicines in a size-dependent manner, Nature Nanotechnology, 7 (2012) 383-388.
[73] E. Pham, M. Yin, C.G. Peters, C.R. Lee, D. Brown, P. Xu, S. Man, L. Jayaraman, E. Rohde, A. Chow, D. Lazarus, S. Eliasof, F.S. Foster, R.S. Kerbel, Preclinical Efficacy of Bevacizumab with CRLX101, an Investigational Nanoparticle-Drug Conjugate, in Treatment of Metastatic Triple-Negative Breast Cancer, Cancer research, 76 (2016) 4493-4503.
[74] S.J. Conley, T.L. Baker, J.P. Burnett, R.L. Theisen, D. Lazarus, C.G. Peters, S.G. Clouthier, S. Eliasof, M.S. Wicha, CRLX101, an investigational camptothecin-containing nanoparticle-drug conjugate, targets cancer stem cells and impedes resistance to antiangiogenic therapy in mouse models of breast cancer, Breast cancer research and treatment, 150 (2015) 559-567.
[75] C.F. Dietrich, M.A. Averkiou, J.M. Correas, N. Lassau, E. Leen, F. Piscaglia, An EFSUMB introduction into Dynamic Contrast-Enhanced Ultrasound (DCE-US) for quantification of tumour perfusion, Ultraschall in der Medizin, 33 (2012) 344-351.
[76] L. Xin, Z. Yan, X. Zhang, Y. Zang, Z. Ding, H. Xue, C. Zhao, Parameters for Contrast-Enhanced Ultrasound (CEUS) of Enlarged Superficial Lymph Nodes for the Evaluation of Therapeutic Response in Lymphoma: A Preliminary Study, Medical science monitor : international medical journal of experimental and clinical research, 23 (2017) 5430-5438.